Geotech Geol Eng (2025) 43:104
https://doi.org/10.1007/s10706-025-03070-w

ORIGINAL PAPER

Evaluating Polymeric Additives for Post-Wildfire Erosion Reduction with Indoor Rainfall Simulation

Alishan Ahmed · Peter R. Robichaud · Amanda K. Hohner · Idil Deniz Akin

Received: 17 May 2024 / Accepted: 27 December 2024

Abstract Critically burnt slopes are treated after a wildfire to reduce erosion and the impacts of eroded soil and ash on downstream water quality. Conventional post-wildfire erosion mitigation methods including mulch, barrier, and seeding treatments have some drawbacks that may result in low efficiency. Polymeric materials, xanthan gum (XG) and polyacrylamide (PAM), are shown to be effective alternatives to the conventional methods in controlling post-wildfire erosion of bare soil. This study evaluates the use of XG and PAM for controlling post-wildfire erosion when the soil surface is covered with hydrophilic ash, which is a common scenario after wildfires in moderate to high soil burn severity regions. Indoor rainfall simulation experiments are performed with soil and ash samples collected after the 2021 Green Ridge Wildfire near Walla Walla, WA to determine the effects of three concentrations (11, 33, and 60 kg/ha) of XG and PAM on infiltration, runoff, and sediment loss in ash-covered soil plots during three wet-dry cycles. Results show that XG and PAM treatments reduce the total sediment loss by up to 68% (XG) and 87% (PAM) during three wetting events for the study soil and ash. Both XG and PAM induce partial surface sealing, which results in higher runoff. However, with subsequent wettings, surface sealing reduces due to redistribution of XG and PAM. The results are explained through the distribution of water along plot depth, scanning electron microscope images, and binding of ash and additives.

Keywords Erosion · Post-wildfire · Biopolymer · Polymer · Wildfire ash

A. Ahmed
WSP USA, Redmond, WA, USA
e-mail: Alishan.Ahmed@wsp.com

P. R. Robichaud
US Department of Agriculture, Forest Service, Rocky Mountain Research Station, Moscow, ID, USA
e-mail: peter.robichaud@usda.gov

A. K. Hohner
Montana State University, Bozeman, MT, USA
e-mail: amanda.hohner@montana.edu

I. D. Akin (✉)
Department of Civil and Environmental Engineering, University of California Los Angeles, Los Angeles, CA 90095, USA
e-mail: idilakin@g.ucla.edu

1 Introduction

Increased erosion on burned slopes is a common cascading impact after a wildfire. For unburned forests, the vegetation canopy reduces the energy of the raindrops, the litter and duff layer protect the underlying soil from raindrop impact and overland flow, and the soil and root cohesion hold the soil together and aids resisting to the detachment and mobilization of soil particles (e.g., Agee 1973; Reubens et al. 2007; Shen et al. 2017). However, after a wildfire the combustion

Published online: 15 January 2025

of protective vegetation and the litter and duff layer exposes the bare soil to raindrops and more importantly overland flow. Direct rainfall energy is transferred from the raindrops to soil particles, which results in more soil detachment (e.g., Shakesby and Doerr 2006). In addition, the combustion of fine roots and reduction in soil cohesion result in a decrease in the resistance of soil against overland flow and mobilization (Gyssels et al. 2005). The eroded soil and ash can move into downstream waterbodies and deteriorate surface water quality and negatively impact aquatic life (e.g., Brito et al. 2021; Smith and Caldwell 2001). Therefore, selected areas are often treated after a wildfire to reduce erosion.

Post-wildfire erosion mitigation treatments can be divided in four broad categories: (i) cover treatments, (ii) chemical treatments, (iii) barrier treatments, and (iv) seeding treatments (Girona-Garcia et al. 2021). Cover treatments include land or aerial application of dry mulch (agricultural straw, wood strands, wood shreds) or hydromulch (e.g., Robichaud et al. 2013). Barrier treatments involve construction of barriers using plant materials (branches, twigs, burnt tree logs, straw wattles, and straw bales) or excavation of trenches to reduce the flow of runoff and intercept the eroded sediment (e.g., Robichaud et al. 2008). In seeding treatments, seeds of fast-growing non-native perennial species such as legumes, grass, rye, and wheat are applied to the burnt slopes to promote quick vegetation recovery (e.g., Badia and Marti 2000). In chemical treatments, polyacrylamide is applied to the burned ground surface (e.g., Inbar et al. 2015; Prats et al. 2014).

A drawback of some cover treatments such as agriculture straw mulch is the inability of mulch to stay on-site during heavy winds (e.g., Vega et al. 2015). Hydromulches bind with soil and therefore can stay on-site, however they decompose quickly (months) and are expensive (Hubbert et al. 2012). Barrier treatments reduce runoff and sediment mobilization but do not prevent soil erosion directly (Robichaud et al. 2008). Seeding treatments do not provide direct and immediate protection against soil erosion and result in environmental concerns related to the introduction of non-native plant species, which may inhibit the regrowth of native vegetation (Beyers 2004; Keeley 2006).

Limited literature exists on the effectiveness of polyacrylamide (PAM) in mitigating post-wildfire soil erosion and the results of the existing studies are contradictory because the effectiveness of PAM depends on several factors such as the type of PAM (anionic, cationic, non-ionic), the rate and method of application, soil type and texture, clay content, cation exchange capacity, concentration of divalent exchangeable cations, and soil water repellency (e.g., Ben-Hur 2006). For instance, Prats et al. (2014) found that 50 kg/ha of PAM application on sandy soil (65% sand, 20% silt, and 15% clay) overlaid by black ash (approximately 88% ground cover) reduced the runoff by 16% but increased the soil loss by 23%. On the contrary, Inbar et al. (2015) found 57% reduction in soil loss with 50 kg/ha of PAM application on soil containing 25% clay, 25% silt, and 50% sand, and no ash cover. Similarly, Akin et al. (2021) conducted indoor rainfall simulation experiments and reported 85% reduction in soil loss with 60 kg/ha of PAM treatment on silty soil. A biopolymer, xanthan gum (XG), was also investigated as another alternative compared to conventional post-wildfire erosion control techniques. For example, Akin et al. (2021) found 64% reduction in erosion of silty soil with 60 kg/ha of XG. Similarly, Movasat and Tomac (2020) reported approximately 92% reduction in erosion of hydrophobic soil with XG.

Limited studies with polymeric treatment alternatives (i.e., PAM and XG) show promising results in terms of reducing erosion. However, most of the existing studies only evaluated the use of polymeric additives on bare soil and the effectiveness was explained through the binding of polymeric additives with soil surfaces. However, immediately after a fire, the ground surface is covered with ash, and therefore, the polymeric additive is applied on the ash layer and first binds with ash particles. Therefore, the effectiveness of additives should be evaluated in the presence of ash. This is especially the case in moderate and high soil burn severity areas, which are often treated to reduce erosion potential. This study evaluates the effectiveness of PAM and XG in reducing erosion in the presence of wildfire ash. Soil and ash samples collected after the 2021 Green Ridge Fire were packed in custom-made plots to obtain a 1-cm thick layer of loose ash on top of burnt soil. XG and PAM were applied on the ash layer in different concentrations. Indoor rainfall simulation experiments were performed on the plots and runoff samples were collected during three wetting events. Collected samples were used to determine runoff rates and sediment loss from untreated and treated plots.

1.1 Study Site

The Green Ridge Fire site is located 30 miles east of Walla Walla, in the Pomeroy Ranger District of Umatilla National Forest, Washington. Lighting started the fire on July 7, 2021, which was contained on October 4, 2021. Over the span of 3 months, the fire burned 18,300 ha. The Burned Area Emergency Response (BAER) teams classified the soil burn severity (SBS) as: 5323 ha of unburned or very low SBS, 9475 ha of low SBS, 3205 ha of moderate SBS, and 297 ha of high SBS (Fig. 1). The digital elevation model (USGS National Map Downloader; https://apps.nationalmap.gov/downloader/) of the study site showed that 22% of the terrain has a slope less than 15°, 58% is between 15° and 30°, and 20% is between 30° and 45°. Soil and ash samples were collected 1 week after the containment of the fire from a region of moderate SBS with a slope of 30°.

2 Materials

2.1 Soil and Ash

The particle size distribution of soil and ash were obtained using a Pario Automated Particle Size Analyzer (Meter Group, Pullman, WA). Loss on Ignition (LOI) was measured by heating the soil at 550 °C for 4 h in a muffle furnace as described by Scalia et al. (2014). Standard methods were used to measure the Atterberg limits (ASTM D4318 2018) and specific gravity (ASTM D792-14 2014). Saturated permeability of soil and ash were measured under constant head in a rigid wall permeability mold having a diameter and height of 10 cm (ASTM D2434-19 2019). The Water Droplet Penetration Time (WDPT) test was performed to evaluate the wettability of soil and ash following Akin and Akinleye (2021). In this test, soil and ash samples were filled in containers of 2-cm diameter and 1-cm height and 10 water droplets were placed on the soil or ash surface in a grid using a standard medicine dropper. The time required for complete penetration of each water droplet was recorded and the average WDPT was calculated to classify the water repellency (King 1981; Chenu et al. 2000).

The zeta potential of soil and ash were measured using a Malvern Zetasizer Nano Z. For zeta potential measurements, 20 mg of oven-dried soil or ash was thoroughly mixed in 50 mL of de-ionized water (0.4 mg/mL) and the suspension was allowed to rest for 30 min to allow the larger particles to settle (e.g., Darrow et al. 2020). The top 10 mL of the supernatant was separated from which 1 mL was transferred to folder capillary zeta cells and the zeta potential was measured. The Cation Exchange Capacity (CEC), soluble cations, and bound cations in soil and ash were measured following standard methods (ASTM D7503 2018). The physical and chemical properties of the soil and ash samples are shown in Table 1.

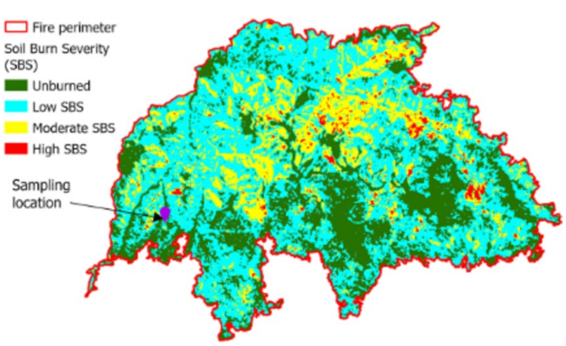

Fig. 1 Soil Burn Severity Map of the 2021 Green Ridge Fire site

2.2 Polymeric Additives

XG is a biopolymer formed by the fermentation of glucose or sucrose by the *Xanthomonas campestris* bacterium (Rosalam and England 2006). The monomer of XG ($C_{35}H_{49}O_{29}$) consists of two glucose, two mannose, and one glucuronic acid (Melton et al. 1976). PAM (monomer: C_3H_5NO) is a synthetic polymer produced by the polymerization of acrylamide or acrylamide and acrylic acid (Doble and Kumar 2005). Purified XG from Sigma-Aldrich (CAS 11138-66-2, St. Louis, MO) and a commercially available PAM (FLOBOND™ A 30, SNF Inc, Riceboro, GA) were used in this study. Both XG and PAM were anionic. The zeta potential of XG was −60.2 mV and the zeta potential of PAM was −79.6 mV.

Table 1 Physical and chemical properties of soil and ash from the 2021 Green Ridge Fire site

Property	Soil				Ash			
Sand size particles (%)	17.7				23.6			
Silt size particles (%)	82.2				76.3			
Clay size particles (%)	0.1				0.1			
Liquid limit	52				50			
Plasticity index	7				15			
USCS classification	MH				–			
Specific gravity	2.66				2.54			
LOI (%)	5.8				16.6			
WDPT (s)	< 1 (hydrophilic)				< 1 (hydrophilic)			
Saturated permeability (cm/s)	1.24×10^{-4}				7.76×10^{-4}			
Zeta potential (mV)	−31.8				−25.4			
CEC (cmol+/kg)	25.8				20.7			
Cations	Ca^{2+}	Mg^{2+}	Na^{+}	K^{+}	Ca^{2+}	Mg^{2+}	Na^{+}	K^{+}
Soluble cations (cmol+/kg)	1.0	0.2	0.1	0.1	1.8	0.8	0.6	6.5
Bound cations (cmol+/kg)	7.8	0.7	–	0.1	8.1	10.4	–	1.9

3 Methods

3.1 Plot Preparation

Rainfall simulation experiments were performed in the rainfall simulation laboratory at the Rocky Mountain Research Station, USDA Forest Service, Moscow, ID. Soil was sieved through a custom-made sieve (opening size of 0.63 cm) in the laboratory to remove gravel and large roots and stems. Plots were prepared following the methods of Pannkuk and Robichaud (2003) and Akin et al. (2021). A schematic of the setup is shown in Fig. 2. Soil was compacted in custom-made metal plot frames with length and width of 68.5 cm, and depth of 7 cm on the front side and 15 cm on the remaining three sides. Soil was compacted in three 3-cm layers at the natural water content of 2.75 ± 0.5% to a void ratio of 2.1.

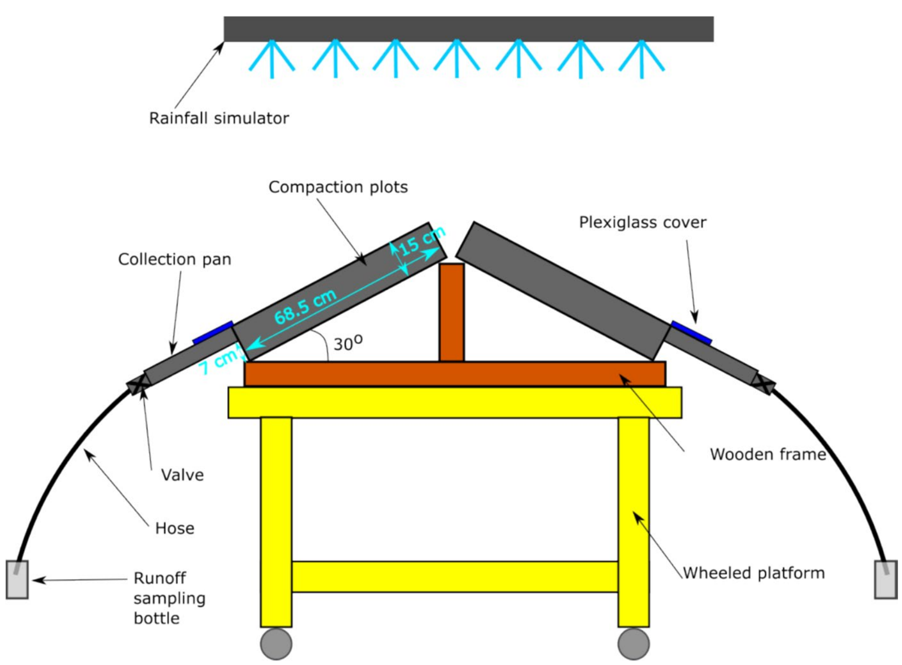

Fig. 2 Schematic of the setup during wetting

The treatment efficiency of XG and PAM was evaluated for scenarios typically observed after a wildfire, where ash is still present on the ground surface. To simulate such field conditions, 0.49 kg of ash was sprinkled on the soil surface forming a loose, 1-cm thick layer. An additional set of plots was prepared without the application of ash on the soil surface (bare soil plots) to evaluate the impacts of ash on runoff and sediment loss. During soil compaction and ash application, a wooden support was clamped on the front edge of the plots as described by Akin et al. (2021), which was removed before the application of rainfall. As a result, 2 cm of unconstrained soil and 1 cm of unconstrained ash were obtained on the front edge. This ensured that the movement of soil and ash with runoff was not interrupted by the front edge of the plots.

Powdered XG or PAM were uniformly sprinkled at three concentrations (11, 33, and 60 kg/ha) on top of the ash layer. In addition, control plots (i.e., untreated) were prepared to obtain baseline data on erosion and runoff. Overall, 8 types of plots were prepared with 2 replicates of each. The 8 plot types include 2 types of untreated plots and 6 types of treated plots. The untreated plots are the bare soil plots (S plots) and soil overlaid with 1 cm thick layer of ash (i.e., ash-covered, A plots). The treated plots include ash-covered plots treated with low (L, 11 kg ha^{-1}), medium (M, 33 kg ha^{-1}), and high (H, 60 kg ha^{-1}) concentrations of XG (i.e., X-L, X-M, and X-H plots) and PAM (P-L, P-M, and P-H plots).

3.2 Rainfall Simulation

All the plots were subjected to three wet-dry cycles. Three wet-dry cycles were selected to evaluate erosion from treated and untreated plots during the first wet season after a wildfire under dry, wet, and partially wet ground conditions (e.g., Robichaud 2000; Akin et al. 2021). For wetting, the plots were transferred to a platform and inclined at 30°. The 30° slope was selected to simulate field conditions as the majority (80%) of the hillslopes at the study site have slopes less than 30°. During each wetting event, the plots were subjected to a rainfall intensity of 100 mm h^{-1} for 30 min to simulate a high intensity storm, which corresponds to a 15-min rainfall of 50 years return period at the study site (Demissie and Mortuza 2015). The rainfall simulator is equipped with VeeJet nozzles that produce raindrops of 3 mm average diameter at a terminal velocity of 8.8 m s^{-1}, providing a potential energy of 275 kJ-ha mm^{-1} at 3 m height (Meyer and Harmon 1979). For drying, plots were placed under two 5700 W ultraviolet light sources on a horizontal platform for 4 h and 8 h after the first and second wetting events, respectively. The drying intervals were selected to simulate the drying between successive rainfalls (e.g., Akin et al. 2021).

3.3 Water Content Sampling

After each wetting and drying event, soil was cored from the plots to measure the water content at three locations along the slope (upslope, midslope, and downslope). Coring was done using a 2-cm diameter steel pipe and each cored soil sample was trifurcated to obtain top, middle, and bottom depth water content. As a result, 9 water content samples (i.e., upslope-top, -middle, -bottom; midslope-top, -middle, -bottom; and downslope-top, -middle, -bottom) were obtained from each plot after each event. This was done to quantify the vertical and spatial distribution of water in the plots.

3.3.1 Runoff Sampling

Runoff from the plots was collected at 5 min intervals during each wetting event. The collected runoff was passed through Whatman Grade 40 filter paper (8 µm pore size) using a Buchner funnel filtration setup. After filtration, the filter papers were oven dried at 105 °C to obtain the mass of sediment loss from the plots. The volume of water obtained after filtration plus the volume of water lost upon oven drying resulted in the runoff volume.

3.3.2 Scanning Electron Microscopy (SEM)

Scanning electron microscopy (SEM) was used to investigate the surface sealing effects of XG and PAM. Dry XG and PAM were mixed with ash to obtain 1:1 (by dry mass) mixtures. The mixtures were saturated with de-ionized water followed by freeze-drying and imaging. SEM images were converted into binary images using ImageJ software (National Institute of Health, Maryland, US) and the fractional area of pores was calculated.

3.3.3 Statistical Analysis

Statistical significance of the results was evaluated using the one-way analysis of variance (ANOVA) at a confidence level of 95%. ANOVA produced a p-value of less than 0.05 which suggests that the probability of the null hypothesis (i.e., no difference in mean values for various groups) to be true was less than 5%. Tukey HSD test was performed to compare the statistically significant difference in the mean values of runoff and sediment loss from untreated and treated plots during each wetting event. Both ANOVA and Tukey HSD tests were performed using R-studio.

4 Results

4.1 Water Content Distribution Post-Wetting

The water content values at upslope, midslope, and downslope locations were averaged to obtain the mean values of top, middle, and bottom water content, denoted as w_{top}, w_{middle}, and w_{bottom}, respectively (Fig. 3). In bare soil plots (i.e., S plots), the water content distribution was uniform along the depth after each wetting event (Fig. 3a). The water content after the first wetting event was $41 \pm 1\%$, and 46% after the second and third wetting event.

In A plots, w_{middle} and w_{bottom} were similar to S plots in the first and second wetting events but the w_{top} values were greater in A plots (Fig. 3b). However, with subsequent wetting events, w_{top} in A plots was reduced from 58% (after wetting 1) to 54% (after wetting 2) to 51% (after wetting 3). The water content in S plots and A plots were similar after the first ($37 \pm 1\%$ for S plots and $35 \pm 1\%$ for A plots) and the second drying events ($37 \pm 0\%$ for S plots and $37 \pm 2\%$ for A plots).

The water content distribution in plots treated with a low concentration of XG and PAM (i.e., X-L and P-L plots) were similar to A plots (Fig. 3c and d). The medium concentration of XG treatment restricted the infiltration of water in the first wetting event (Fig. 3e). The w_{top} value (47%) was higher than w_{middle} (40%), which was higher than w_{bottom} (28%). However, with subsequent wettings, the difference in w_{top}, w_{middle}, and w_{bottom} was reduced and after the third wetting event, w_{top}, w_{middle}, and w_{bottom} values were 49%, 46%, and 44% respectively. The medium concentration of PAM treatment also resulted in restricted flow of water along the plots' depth. The effects of PAM on infiltration were less pronounced than XG in the beginning, but were observed even after the second wetting event, where w_{top} was 48% and w_{bottom} was 39% (Fig. 3f). Similarly, the high concentration of XG also restricted the infiltration of water and the difference in top, middle, and bottom water content was even higher after the first wetting event (w_{top}, w_{middle}, and w_{bottom} values were 54%, 35%, and 12%, respectively). The difference in the water content along the plots' depth was reduced with subsequent wettings (Fig. 3g). At a high concentration, PAM also restricted the infiltration of water, but the water contents were greater than X-H plots. The effects of PAM on water infiltration were observed after both first and second wetting events (Fig. 3h).

4.2 Time to Runoff and Sediment Loss

In the first wetting event, negligible runoff (< 100 mL) and sediment loss (< 2 g) were generated from S plots and A plots (Fig. 4). In the second wetting event, runoff and sediment loss started within 5 min from S plots and within 10 min from A plots, while in the third wetting event, runoff and sediment loss started within 5 min from both S and A plots. In the first wetting event, the plots treated with low concentration of XG and PAM generated runoff and sediment loss after 20 min. The medium concentration of XG and PAM treatment resulted in runoff and sediment loss generation after 15 min (for X-M plots) and 20 min (for P-M plots). When applied at a high concentration (i.e., 60 kg ha^{-1}), XG and PAM treatments resulted in runoff and sediment loss generation after 10 min (for X-H plots) and 15 min (for P-H plots). In the second and third wetting events, runoff and sediment loss from plots treated with all concentrations of XG and PAM started within 5 min.

4.3 Cumulative Runoff and Sediment Loss

S plots and A plots generated negligible runoff (< 100 mL) and sediment loss (< 2 g) in the first wetting event. The cumulative runoff from S plots in the second wetting event was 8.3 L and the cumulative sediment loss was 910 g (Fig. 5). The presence of ash in the A plots resulted in 25% reduction in cumulative runoff and 56% reduction in sediment loss compared

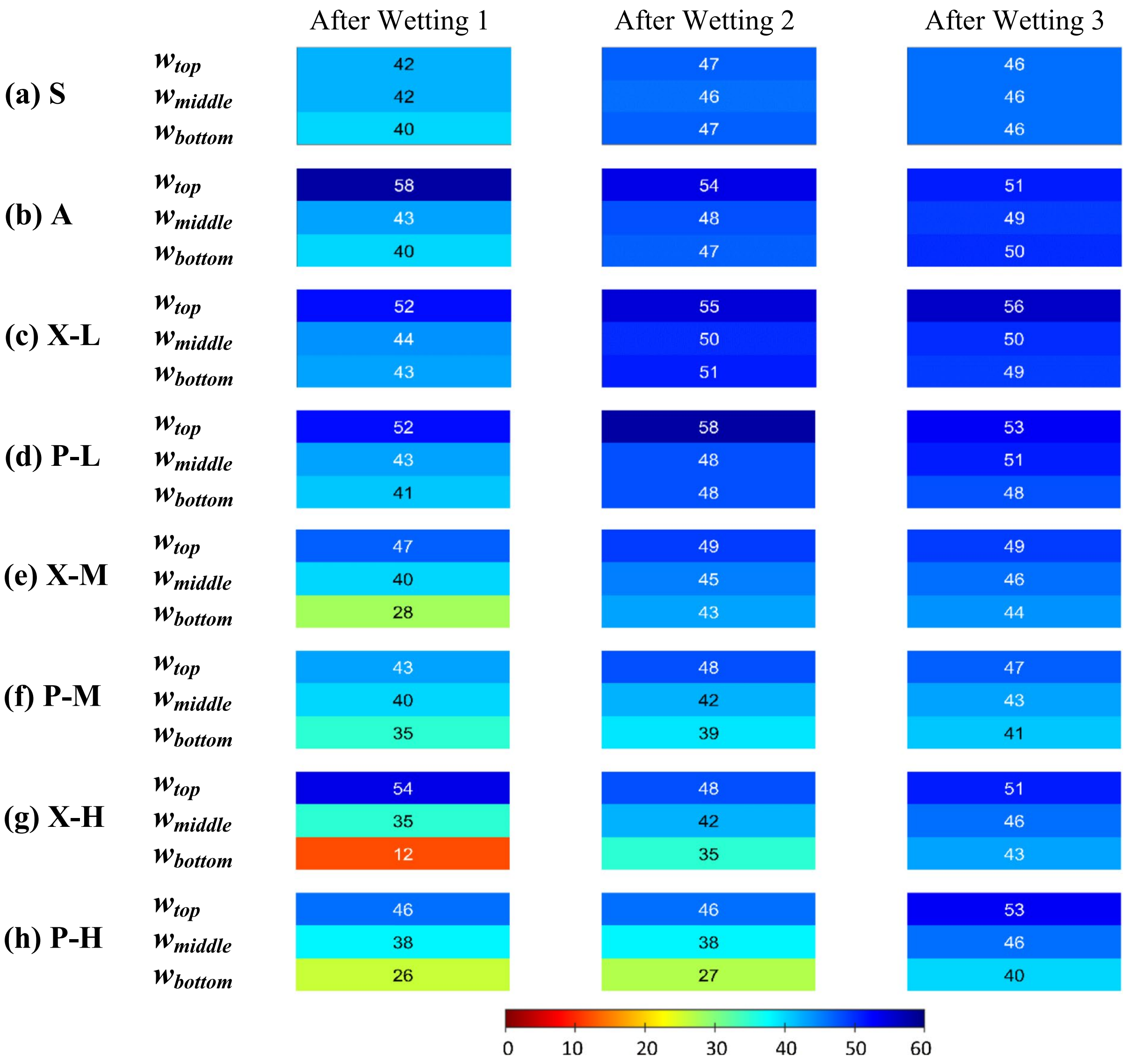

Fig. 3 Average water contents (%) after each wetting event at the top depth (w_{top}), middle depth (w_{middle}), and bottom depth (w_{bottom}) of the plots

to S plots. In the third wetting event, the cumulative runoff from S and A plots were similar (9.4 L from S plots and 9.3 L from A plots). However, the sediment loss from A plots was 30% less than S plots.

In the first wetting event, only 4% (for X-L plots) and 5% (for P-L plots) of rainfall was not infiltrated into the plots and turned into runoff. The cumulative runoff was 1.0 L from X-L plots and 1.3 L from P-L plots and the cumulative sediment loss from both X-L and P-L plots was only 9 g. In the second wetting event, the cumulative runoff from X-L and P-L plots were 3% and 11% less than A plots, respectively, and the cumulative sediment loss from X-L plots was 52% less and from P-L plots was 78% less than A plots. In the third wetting event, the cumulative runoff from X-L plots was 10% lower and from P-L plots was 11% lower than A plots. The cumulative sediment loss from X-L and P-L plots was 9% and 53% lower than A plots. Overall, the total cumulative runoff (i.e., cumulative runoff due to first, second, and third wetting event combined) from X-L and P-L plots was similar to the control plots (1% lower for X-L plots

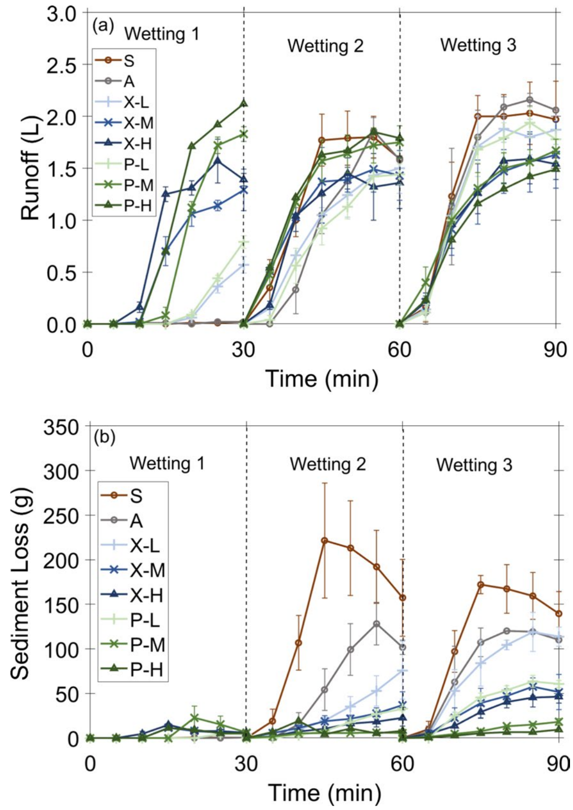

Fig. 4 Runoff (**a**), and sediment loss (**b**) from the plots during wetting events

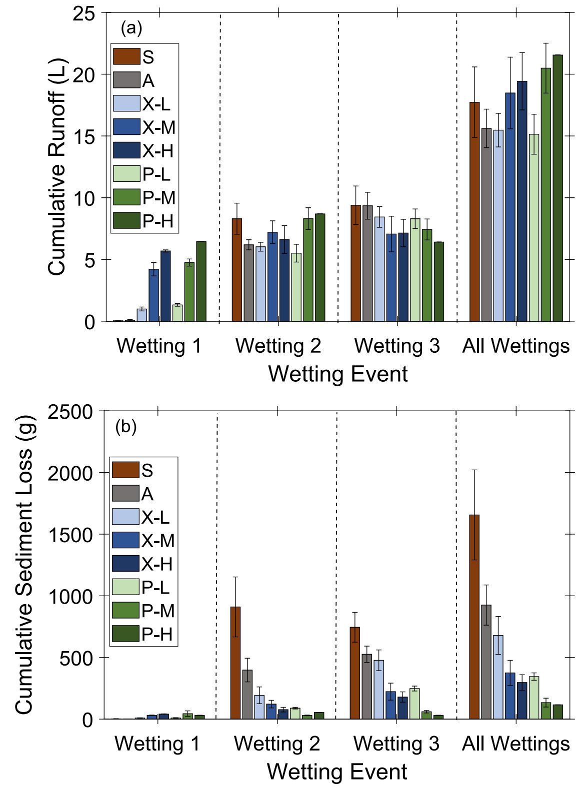

Fig. 5 Mean cumulative runoff (**a**) and mean cumulative sediment loss (**b**) after wetting events

and 3% lower for P-L plots), and the total cumulative sediment loss (i.e., sediment loss due to first, second, and third wetting event combined) decreased by 27% (for XG) and 63% (for PAM). For both X-L and P-L plots, runoff was not significantly different than A plots in all three wetting events ($p > 0.05$). For X-L plots, sediment loss was not significantly different than A plots in three wetting event ($p > 0.05$) while for P-L plots, sediment loss was significantly lower than the A plots only in the second wetting event ($p < 0.05$).

The cumulative runoff from X-M plots was 4.2 L (18% of the applied rainfall) and from P-M plots was 4.8 L (20% of the applied rainfall) in the first wetting event and the cumulative sediment loss was only 31 g from X-M plots and 44 g from P-M plots. In the second wetting event, the cumulative runoff was 17% higher from X-M plots and 34% higher from P-M plots as compared to A plots. Despite higher runoff, the sediment loss from X-M and P-M plots was 69% and 93% lower than A plots, respectively. In the third wetting event, the respective cumulative runoff from X-M and P-M plots was 25% and 21% lower than the control plots and the cumulative sediment loss was 58% lower from X-M plots and 89% lower from P-M plots relative to A plots. Over the three wetting events, 33 kg ha^{-1} of XG and PAM treatment increased the total cumulative runoff by 18% (for XG) and 31% (for PAM) and reduced the total cumulative sediment loss by 59% (for XG) and 86% (for PAM). Tukey HSD tests showed that the runoff from X-M and P-M plots was not significantly higher than A plots in the three wetting events ($p > 0.05$). Further, sediment loss from both X-M and P-M plots was significantly lower than A plots in the second and third wetting events ($p < 0.01$).

The high concentration (60 kg ha^{-1}) of XG and PAM treatment resulted in 5.7 L (from X-H plots) and 6.5 L (from P-H plots) of runoff in the first wetting event and the cumulative sediment loss was only 41 g from X-H plots and 31 g from P-H plots. In the second wetting event, the cumulative runoff was 7% higher from X-H plots and 40% higher from P-H plots but the cumulative sediment loss was 81% lower (for X-H) and 86% lower (for P-H) compared to A plots. The cumulative runoff from X-H and P-H plots in the third wetting event was 24% and 31% lower than A plots, respectively. Moreover, the cumulative sediment loss was reduced by 66% (for X-H) and 94% (for P-H). Overall, due to the application of 60 kg/ha of XG and PAM, the total cumulative runoff increased by 24% (for X-H) and 38% (for P-H), and the total cumulative sediment loss reduced by 68% (for X-H) and 87% (for P-H). For X-H and P-H plots, the runoff was not significantly higher than A plots in the three wetting events according to the Tukey HSD test ($p \nless 0.05$). However, X-H and P-H plots produced significantly lower sediment loss in second and third wetting event ($p < 0.01$ for X-H plots in second wetting and for P-H in second and third wetting and $p < 0.05$ for X-H plots in third wetting event).

5 Discussion

5.1 Impacts of Ash on Runoff and Sediment Loss

In the first wetting event, negligible runoff and sediment loss were obtained from S plots and A plots because the applied rainfall increased the saturation of initially dry soil (in S plots) and soil and ash (in A plots). The ash layer retained more water, which was indicated by higher w_{top} in A plots (58%) compared to S plots (42%). However, ash did not inhibit the flow of water into the soil as evidenced by similar w_{middle} (42% for S and 43% for A plots) and w_{bottom} (40% for both S and A plots). The impact of ash on infiltration immediately after a fire depends on various factors such as the type of ash, degree of soil water repellency, hydraulic conductivity of soil and ash, and soil texture (e.g., Eteigni and Campbell 1991, Onda et al. 2008, Woods and Balfour 2008, 2010). Several studies have found that ash can reduce infiltration by clogging soil pores and forming hydraulically smoother surface (e.g., Mallik et al. 1984; Onda et al. 2008). However, some studies have also shown that ash can intercept and store rainfall and result in increased infiltration (e.g., Woods and Balfour 2008; Larsen et al. 2009, Bodi et al. 2014). If unsaturated hydrophilic ash is present on top of soil, the applied rainfall increases the saturation of ash and if the permeability of the underlying soil is lower than ash, ponding can occur at the ash-soil interface and saturation excess overland flow may occur in the ash layer over the soil layer (Bodi et al. 2014). Since the permeability of ash and soil used in this study were of the same order of magnitude (7.76×10^{-4} cm s^{-1} for ash and 1.24×10^{-4} cm s^{-1} for soil), saturation excess overland flow was not observed, and the rainfall infiltrated into the soil after saturating the ash layer (Fig. 3b).

After the first drying event, the water content of S plots and A plots were similar (37 ± 1% for S plots and 35 ± 1% for A plots) however, runoff generation from A plots was delayed by 5 min in the second wetting event. This observation may be because of the additional water required to saturate the ash layer. Woods and Balfour (2008) also showed that the presence of ash on top of soil results in a delay in runoff generation and the time to runoff is a function of the thickness of ash layer. Because the ash layer retains more water, the cumulative runoff from A plots was 25% lower than S plots. As a result of reduced runoff and protection of underlying soil from rainsplash erosion by the ash layer, the cumulative sediment loss decreased 56%. Reduced sediment loss due to the presence of ash has also been reported by previous studies (e.g., Leighton-Bayce et al. 2007, Cerdà and Doerr 2008, Woods and Balfour 2008).

At the end of the second wetting event, w_{top} in A plots was 54% (4% lower than the first wetting event), which was attributed to redistribution of ash. Spatial and vertical redistribution of ash is common shortly after a fire due to wind, water, free-thaw cycles, and bioturbation (e.g., Czimczik and Masiello 2007; Cerdà and Doerr 2008; Topoliantz et al. 2006). In this study, the redistribution occurred due to the applied rainfall and some of the ash moved with the runoff, while some ash migrated into the soil. The difference in w_{top} in A plots (54%) and S plots (47%) after the second wetting event suggests that some ash was still present on the plots. Moreover, the cumulative sediment loss from A plots in the second wetting event was 398 g, which is less than the amount of ash applied on the plots (i.e., 490 g). This observation also suggests that some ash was still present on A plots after the second wetting event.

In the third wetting event, the runoff and sediment loss from both S and A plots started within 5 min because of reduced ash content in A plots. The average water content in the S and A plots after the second drying event were very similar (37 ± 0% for S plots and 37 ± 2% for A plots), which also suggests that due to reduced ash content, no additional water was required to saturate the A plots and consequently, the cumulative runoff from both S and A plots was also similar in the third wetting event. However, despite having similar runoffs, the cumulative sediment loss from A plots was 30% lower than S plots, which may be attributed to vertical redistribution of ash.

5.2 XG and PAM Treatment for Erosion Control

Application of XG and PAM treatment at all concentrations resulted in earlier runoff generation, and the time to runoff in the first wetting event decreased with the increase in treatment concentrations. For instance, runoff started within 20 min from X-L plots, 15 min from X-M plots, and 10 min from X-H plots. A similar trend was observed for PAM-treated plots. In the second and third wetting event, runoff started within 5 min from all XG- and PAM-treated plots. Even though ash was also present in the treated plots, the application of XG and PAM on top of the ash layer had an inverse effect on the time to runoff compared to A plots, particularly in the first and second wetting events. The early generation of runoff from the treated plots in the first wetting event was attributed to the surface sealing effects of XG and PAM. The water content distributions in the treated plots suggest that XG and PAM restricted the infiltration of water into the plots. After the first wetting event, w_{top} values in treated plots were greater than w_{middle}, which were greater than w_{bottom}. The difference between w_{top} and w_{bottom} increased with increasing additive concentration and the difference was generally higher for XG-treated plots than PAM-treated plots (9% for X-L, 19% for X-M, 42% for X-H, 11% for P-L, 8% for P-M, 20% for P-H). The middle and bottom water contents in all the treated plots were greater than the initial water content (2.75 ± 0.5%), suggesting that the additives did not seal the surface completely and water was able to infiltrate into the plots.

Both XG and PAM form hydrogel upon wetting and the hydrophilic functional groups of the hydrogel structure retain water which results in swelling (e.g., De et al. 2002; Qureshi et al. 2017). The swelled hydrogel structure on the surface causes reduction in infiltration (e.g., Akin et al. 2021). In addition, both XG and PAM increase the viscosity of infiltrating water which results in reduction in the hydraulic conductivity of soil (e.g., Bouazza et al. 2009; Wiszniewski and Cabalar 2014). The SEM images were used to calculate the fractional area of pores that relates to surface sealing effects of XG and PAM (Fig. 6). The fractional area of pores for XG-ash mixtures varied between 12 and 23% while for PAM-ash mixtures the range was between 25 and 29%. The lower porosity of XG-ash mixtures suggests that XG induces greater surface sealing than PAM, which explains the greater difference between w_{top} and w_{bottom} in XG- treated plots than PAM-treated plots.

The effects of reduced infiltration in the first wetting event were also reflected in the runoff volume. The cumulative runoff from treated plots increased with increasing additive concentration (1.0 L for X-L, 4.2 L for X-M, 5.7 L for X-H, 1.3 L for P-L, 4.8 L for P-M, and 6.5 L for P-H). For all concentrations, the cumulative runoff was more for PAM-treated plots than XG-treated plots even though XG induced greater surface sealing. Higher w_{top} values in XG-treated plots compared to PAM-treated plots indicate that XG retained more water, which resulted in relatively lower runoffs from XG-treated plots. Despite runoff generation in the first wetting event, the treated plots produced less than 50 g of sediment loss. This finding is likely because both XG and PAM bonded with ash particles and reduced the raindrop impact and subsequent particle detachment. Both additives used in this study were anionic and bonded with the ash particles through cation bridging (e.g., Mpofu et al. 2003; Lee et al. 2012). The divalent cations (e.g., Ca^{2+} and Mg^{2+}) present as bound cations on the surface of ash particles and as soluble cations in the pore water reduce the electrostatic repulsion between the negatively charged ash particles and anionic polymers and bridge or anchor them together (Theng 1982, 2012).

The surface sealing effects of XG were reduced after the second wetting event as evidenced by the reduction in the difference in w_{top} and w_{bottom} (4% for X-L, 6% for X-M, 13% for X-H). The reduction in surface sealing was attributed to the redistribution of XG with runoff and into the soil. The cumulative runoff from X-L plots was similar to A plots (3% lower) while from X-M and X-H plots, the cumulative runoff was higher than A plots (16% higher for X-M and 7%

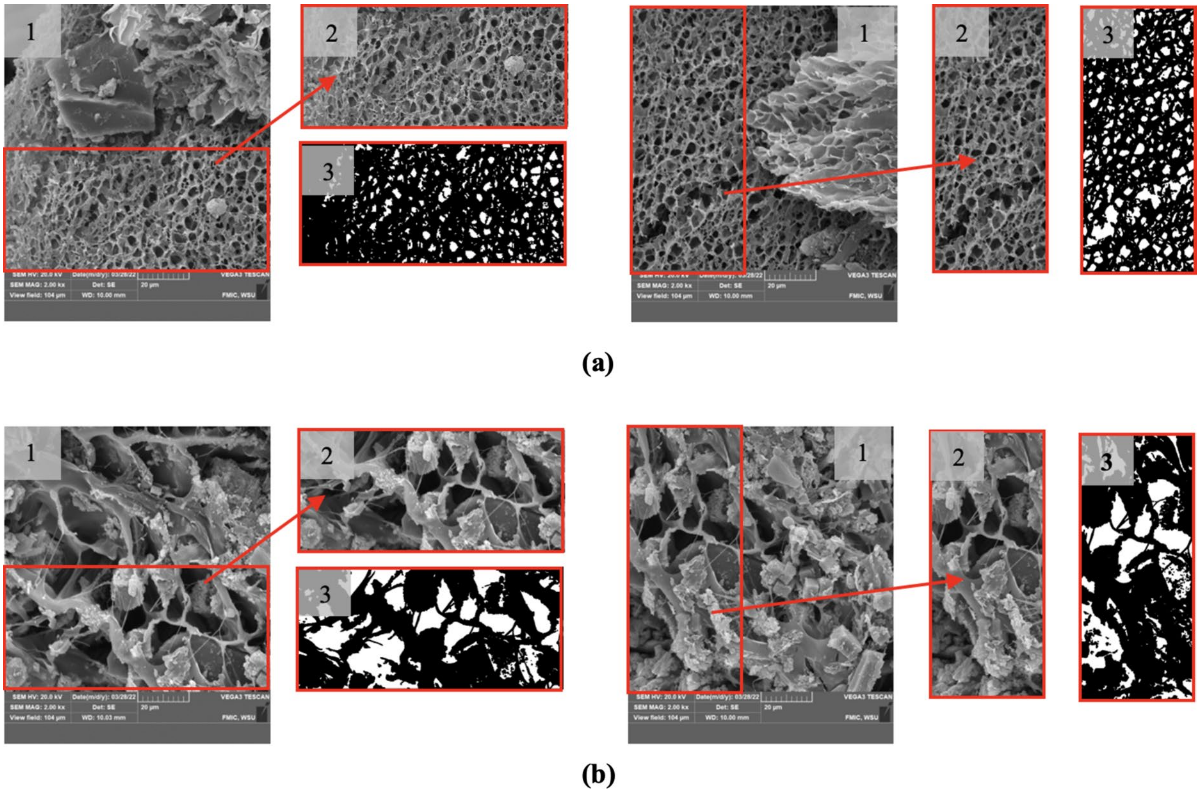

Fig. 6 Microimages of 1:1 (w/w) mixtures of XG and ash (**a**) and PAM and ash (**b**). Images 1: scanning electron microscope (SEM) images, Images 2: part of SEM images converted into binary images, Images 3: binary images used to calculate the fractional area of pores

higher from X-H). In addition, the cumulative sediment loss from all XG-treated plots was less than A plots (sediment loss reduced by 52% for X-L, 69% for X-M, and 81% for X-H). Higher runoff and lower sediment loss indicates that all the applied XG mass was not lost from the plots after first and second wetting events. In PAM-treated plots, the water content distributions after the second wetting event were similar to the first wetting event, which suggests that the surface sealing effects of PAM were similar after the first and second wetting events and the redistribution of PAM was less than XG. As a result, the cumulative runoffs from PAM-treated plots were higher than A plots, as well as XG-treated plots (34% higher for P-M and 40% higher from P-H). Moreover, the cumulative sediment loss from PAM-treated plots was less than A plots and XG-treated plots (sediment loss reduced by 78% for P-L, 93% for P-M, and 86% for P–H), which suggests that PAM provided stronger binding of ash particles than XG. The negative surface potential of PAM (−79.6 mV) was greater than XG (−60.2 mV) which indicates that the interaction of PAM with the cations present on the surface of ash particles was higher than XG which resulted in stronger cation bridging between PAM and ash particles.

The third wetting event resulted in further redistribution of XG and PAM and reduced surface sealing effects as indicated by the water content distributions. The cumulative runoff was lower from the treated plots compared to A plots (runoff reduced by 10% for X-L, 25% for X-M, 24% for X-H, 11% for P-L, 21% for P-M, 31% for P-H). This is likely because: (1) A plots had greater runoff in the third wetting event due to the redistribution of ash, which retained more water and reduced runoff in the first and second wetting event, (2) the redistribution of XG and PAM from the surface of plots exposed the ash layer, which retained more water and reduced runoff, and (3) XG and PAM that migrated into the plots increased the water retention in soil (e.g., Sojka et al. 1998; Tran et al. 2018; Chen et al. 2019). The sediment loss from all treated plots was lower than A plots (sediment loss reduced by 9% for X-L, 58% for X-M, 66% for X-H, 53% for P-L, 89% for P-M, 94% for P-H). The reduction in sediment loss was attributed to the combined effect of reduced runoff and binding of ash and soil by XG and PAM.

The overall effects of the low concentration of XG and PAM treatments due to three wet-dry cycles include a marginal reduction in total cumulative runoff (1% for XG and 3% for PAM), and 27% (for XG) and 63% (for PAM) reduction in total sediment loss. This observation suggests that even a small concentration of XG or PAM may reduce post-wildfire erosion in the presence of ash without increasing runoff. Upon increasing the treatment concentration from low to medium, even though the total cumulative runoff increased (15% more runoff for XG and 31% for PAM relative to A plots), a further reduction in erosion was also achieved (total cumulative sediment reduced by 59% for XG and 86% for PAM). However, increasing the XG and PAM concentrations to 60 kg/ha resulted in increased total cumulative runoff (24% for XG and 38% for PAM) while providing only 9% (for XG) and 1% (for PAM) additional erosion control. This suggests that 11 and 33 kg/ha of XG and PAM treatment can provide considerable erosion reduction (27–59% for XG and 63–86% for PAM) over three wet-dry cycles and increasing the treatment concentration to 60 kg/ha may not provide additional benefits. The results also showed that PAM provided more erosion reduction than XG for all concentrations. For example, a similar reduction in total sediment loss was achieved with 11 kg/ha of PAM and 33 kg/ha of XG.

Overall, the rainfall simulation experiments conducted in laboratory conditions showed that both XG and PAM can reduce erosion. However, field experiments are necessary before the methods are implemented because field conditions such as soil and ash properties, thickness of the ash layer, rainfall characteristics, and slope angle may show variations.

6 Conclusions

The use of XG and PAM for reducing post-wildfire erosion in the presence of wildfire ash was evaluated through laboratory-scale rainfall simulation experiments. The results suggest that both XG and PAM can seal the ash surface and reduce water infiltration. The surface sealing effects increase as the concentration of XG or PAM increases. The surface sealing effect of XG was more pronounced than PAM for all concentrations in the first wetting event but was reduced in the second wetting event due to the redistribution of XG. PAM was more stable on the plots and induced surface sealing in both the first and the second wetting events, resulting in higher runoff compared to control and XG-treated plots. During the third wetting event, the surface sealing effects of XG and PAM were absent and the runoffs from treated plots were less than the control plots (10–24% less from XG-treated plots and 11–31% less from PAM-treated plots). Overall, compared to control plots, the total runoff was 1% lower from low-concentration, 18% higher from medium concentration, and 24% higher from high concentration XG-treated plots. The low concentration of PAM treatment had a negligible effect on the total runoff (3% lower), but medium and high concentrations of PAM increased the total runoff by 31% and 38%, respectively. Both XG and PAM reduced the total sediment loss, however due to a possibly stronger interaction between PAM and ash particles, the sediment loss from PAM-treated plots was lower than XG-treated plots for all concentrations. XG reduced the total sediment loss by 27%, 59%, and 68% when applied at low, medium, and high concentrations, respectively. The total sediment loss was reduced by 63% with low, 86% with medium, and 87% with high concentration of PAM. These laboratory results suggest that additional research is warranted at the hillslope scale.

Acknowledgements This work has been funded in part by State of Washington Water Research Center and US Department of Agriculture, Forest Service, Rocky Mountain Research Station. We thank the sponsors for their support.

Funding State of Washington Water Research Center, Washington State University

Data Availability Enquiries about data availability should be directed to the authors.

Declarations

Conflict of interest The authors have no competing interests to declare that are relevant to the content of this article.

References

Agee J (1973) Prescribed fire effects on physical and hydrologic properties of mixed-conifer forest floor and soil. In: Water Res. Center, Univ. Calif. Contrb. Report, 143:57

Akin ID, Akinleye TO (2021) Water vapor sorption behavior of wildfire-burnt soil. J Geotech Geoenviron Eng 147:4021115

Akin ID, Garnica SS, Robichaud PR, Brown RE (2021) Surficial stabilization of wildfire-burnt hillslopes using xanthan gum and polyacrylamide. Geotech Geol Eng. https://doi.org/10.1007/s10706-021-01951-4

ASTM D2434 (2019). Standard test method for permeability of granular soils (Constant Head). ASTM

ASTM D4318 (2018). Standard test methods for liquid limit, plastic limit, and plasticity index of soils. ASTM

ASTM D7503 (2018). Standard test method for measuring the exchange complex and cation exchange capacity of inorganic fine-grained soils. ASTM

ASTM D792-14 (2014). Standard test methods for specific gravity of soil solids by water pycnometer. ASTM

Badia D, Marti C (2000) Seeding and mulching treatments as conservation measures of two burned soils in the central ebro valley, NE Spain. Arid Soil Res Rehabil 14(3):219–232. https://doi.org/10.1080/089030600406635

Ben-Hur M (2006) Using synthetic polymers as soil conditioners to control runoff and soil loss in arid and semi-arid regions. Rev Soil Res 44(3):191–204. https://doi.org/10.1071/SR05175

Beyers JL (2004) Postfire seeding for erosion control: effectiveness and impacts on native plant communities. Conserv Biol 18(4):947–956. https://doi.org/10.1111/j.1523-1739.2004.00523.x

Bodí MB, Martin DA, Balfour VN, Santín C, Doerr SH, Pereira P, Cerdà A, Mataix-Solera J (2014) Wildland fire ash: production, composition and eco-hydro-geomorphic effects. Earth Sci Rev 130:103–127. https://doi.org/10.1016/j.earscirev.2013.12.007

Bouazza A, Gates WP, Ranjith PG (2009) Hydraulic conductivity of biopolymer-treated silty sand. Géotechnique 59(1):71–72. https://doi.org/10.1680/geot.2007.00137

Brito DQ, Santos L, Passos C, Oliveira-Filho EC (2021) Short-term effects of wildfire ash on water quality parameters: a laboratory approach. Bull Environ Contam Toxico 107(3):500–505

Cerdà A, Doerr SH (2008) The effect of ash and needle cover on surface runoff and erosion in the immediate post-fire period. CATENA 74(3):256–263. https://doi.org/10.1016/j.catena.2008.03.010

Chen C, Wu L, Perdjon M, Huang X, Peng Y (2019) The drying effect on xanthan gum biopolymer treated sandy soil shear strength. Constr Build Mater 197:271–279. https://doi.org/10.1016/j.conbuildmat.2018.11.120

Chenu C, Le Bissonnais Y, Arrouays D (2000) Organic matter influence on clay wettability and soil aggregate stability. Soil Sci Soc Am J 64(4):1479–1486. https://doi.org/10.2136/sssaj2000.6441479x

Czimczik CI, Masiello CA (2007) Controls on black carbon storage in soils. Global Biogeochem Cycles 21:GB3005. https://doi.org/10.1029/2006GB002798

Darrow MM, Guo R, Trainor TP (2020) Zeta potential of cation-treated soils and its implication on unfrozen water mobility. Cold Regions Sci Technol 173:103029. https://doi.org/10.1016/j.coldregions.2020.103029

De SK, Aluru NR, Johnson B, Crone WC, Beebe DJ, Moore J (2002) Equilibrium swelling and kinetics of pH-responsive hydrogels: models, experiments, and simulations. J Microelectromech Syst 11:544–555. https://doi.org/10.1109/JMEMS.2002.803281

Demissie Y, Mortuza MR (2015) Updated and forward looking rainfall and runoff intensity- duration-frequency curves for Washington state, In: 6th Annual Pacific Northwest Climate Science Conference, Coeur d'Alene, ID, Nov. 3–5

Doble M, Kumar A (2005) Biotreatment of industrial effluents. Elsevier, Amsterdam

Etiegni L, Campbell AG (1991) Physical and chemical characteristics of wood ash. Biores Technol 37(2):173–178

Girona-García A, Vieira DCS, Silva J, Fernández C, Robichaud PR, Keizer JJ (2021) Effectiveness of post-fire soil erosion mitigation treatments: a systematic review and meta-analysis. Earth Sci Rev 217:103611. https://doi.org/10.1016/j.earscirev.2021.103611

Gyssels G, Poesen J, Bochet E, Li Y (2005) Impact of plant roots on the resistance of soils to erosion by water: a review. Prog Phys Geogr Earth Environ 29(2):189–217. https://doi.org/10.1191/0309133305pp443ra

Hubbert KR, Wohlgemuth PM, Beyers JL (2012) Effects of hydromulch on post-fire erosion and plant recovery in chaparral shrublands of southern California. Int J Wildland Fire 21(2):155–167. https://doi.org/10.1071/WF10050

Inbar A, Ben-Hur M, Sternberg M, Lado M (2015) Using polyacrylamide to mitigate post-fire soil erosion. Geoderma 239–240:107–114. https://doi.org/10.1016/j.geoderma.2014.09.026

Keeley JE (2006) Fire management impacts on invasive plants in the western United States. Conserv Biol 20(2):375–384. https://doi.org/10.1111/j.1523-1739.2006.00339.x

King PM (1981) Comparison of methods for measuring severity of water repellence of sandy soils and assessment of some factors that affect its measurement. Aust J Soil Res 19(3):275–328

Larsen IJ, MacDonald LH, Brown E, Rough D, Welsh MJ, Pietraszek JH, Libohova Z, Dios Benavides-Solorio J, Schaffrath K (2009) Causes of post-fire runoff and erosion: water repellency, cover, or soil sealing? Soil Sci Soc Am J 73(4):1393–1407. https://doi.org/10.2136/sssaj2007.0432

Lee BJ, Schlautman MA, Toorman E, Fettweis M (2012) Competition between kaolinite flocculation and stabilization in divalent cation solutions dosed with anionic polyacrylamides. Water Res 46(17):5696–5706. https://doi.org/10.1016/j.watres.2012.07.056

Leighton-Boyce G, Doerr SH, Shakesby RA, Walsh RPD (2007) Quantifying the impact of soil water repellency on overland flow generation and erosion: a new approach using rainfall simulation and wetting agent on in situ soil. Hydrol Process 21(17):2337–2345. https://doi.org/10.1002/hyp.6744

Mallik AU, Gimingham CH, Rahman AA (1984) Ecological effects of heather burning: I. water infiltration, moisture retention and porosity of surface soils. J Ecol 72:767–776. https://doi.org/10.2307/2259530

Melton LD, Mindt L, Rees DA (1976) Covalent structure of the extracellular polysaccharide from *Xanthomonas campestris*: evidence from partial hydrolysis studies. Carbohydr Res 46(2):245–257. https://doi.org/10.1016/S0008-6215(00)84296-2

Meyer LD, Harmon WC (1979) Multiple-intensity rainfall simulator for erosion research on row sideslopes. Trans ASAE 22(1):100–0103

Movasat M, Tomac I (2020) Post-Fire mudflow prevention by biopolymer treatment of water repellent slopes. Geo-Congress 2020, pp 170–178. https://doi.org/10.1061/9780784482834.019

Mpofu P, Addai-Mensah J, Ralston J (2003) Investigation of the effect of polymer structure type on flocculation, rheology and dewatering behaviour of kaolinite dispersions. Int J Miner Process 71(1):247–268. https://doi.org/10.1016/S0301-7516(03)00062-0

Onda Y, Dietrich WE, Booker F (2008) Evolution of overland flow after a severe forest fire, Point Reyes California. Catena 72(1):13–20

Pannkuk CD, Robichaud PR (2003) Effectiveness of needle cast at reducing erosion after forest fires. Water Resour Res. https://doi.org/10.1029/2003WR002318

Prats SA, dos Santos Martins MA, Malvar MC, Ben-Hur M, Keizer JJ (2014) Polyacrylamide application versus forest residue mulching for reducing post-fire runoff and soil erosion. Sci Total Environ 468–469:464–474. https://doi.org/10.1016/j.scitotenv.2013.08.066

Qureshi MU, Chang I, Al-Sadarani K (2017) Strength and durability characteristics of biopolymer-treated desert sand. Geomech Eng 12(5):785–801

Reubens B, Poesen J, Danjon F, Geudens G, Muys B (2007) The role of fine and coarse roots in shallow slope stability and soil erosion control with a focus on root system architecture: a review. Trees Struct Funct 21(4):385–402. https://doi.org/10.1007/s00468-007-0132-4

Robichaud PR (2000) Fire effects on infiltration rates after prescribed fire in Northern Rocky Mountain forests USA. J Hydrol 231–232:220–229. https://doi.org/10.1016/S0022-1694(00)00196-7

Robichaud PR, Pierson FB, Brown RE, Wagenbrenner JW (2008) Measuring effectiveness of three postfire hillslope erosion barrier treatments western Montana USA. Hydrol Process 22(2):159–170. https://doi.org/10.1002/hyp.6558

Robichaud PR, Lewis SA, Wagenbrenner JW, Ashmun LE, Brown RE (2013) Post-fire mulching for runoff and erosion mitigation: Part I: Effectiveness at reducing hillslope erosion rates. Catena 105:75–92. https://doi.org/10.1016/j.catena.2012.11.015

Rosalam S, England R (2006) Review of xanthan gum production from unmodified starches by *Xanthomonas comprestris* sp. Enzyme Microb Technol 39(2):197–207. https://doi.org/10.1016/j.enzmictec.2005.10.019

Scalia J, Benson C, Bohnhoff G, Edil T, Shackelford C (2014) Long-term hydraulic conductivity of a bentonite-polymer composite permeated with aggressive inorganic solutions. J Geotech Geoenviron Eng. https://doi.org/10.1061/(ASCE)GT.1943-5606.0001040

Shakesby RA, Doerr SH (2006) Wildfire as a hydrological and geomorphological agent. Earth Sci Rev 74(3–4):269–307

Shen P, Zhang LM, Chen HX, Gao L (2017) Role of vegetation restoration in mitigating hillslope erosion and debris flows. Eng Geol 216:122–133. https://doi.org/10.1016/j.enggeo.2016.11.019

Smith CJ, Caldwell J (2001) Salmon and steelhead habitat limiting factors in the Washington coastal streams of WRIA 21, Water Resources Inventory Area 21 Final report, Washington State Conservation Commission, 300 Desmond Drive, Lacey, WA 98503

Sojka RE, Lentz RD, Ross CW, Trout TJ, Bjorneberg DL, Aase JK (1998) Polyacrylamide effects on infiltration in irrigated agriculture. J Soil Water Conserv 53(4):325–331

Theng BKG (1982) Clay-polymer interactions: summary and perspectives. Clays Clay Miner 30(1):1–10. https://doi.org/10.1346/CCMN.1982.0300101

Theng BKG (2012) Formation and properties of clay-polymer complexes. Elsevier, Amsterdam

Topoliantz S, Ponge J-F, Lavelle P (2006) Humus components and biogenic structures under tropical slash-and-burn agriculture. Eur J Soil Sci 57:269–278

Tran ATP, Cho GC, Lee SJ, Chang I (2018) Effect of xanthan gum biopolymer on the water retention characteristics of unsaturated sand. In: International Conference on Unsaturated Soil. ISSMGE

Vega JA, Fernández C, Fonturbel T (2015) Comparing the effectiveness of seeding and mulching+seeding in reducing soil erosion after a high severity fire in Galicia (NW Spain). Ecol Eng 74:206–212. https://doi.org/10.1016/j.ecoleng.2014.10.019

Wiszniewski M, Cabalar AF (2014) Hydraulic conductivity of a biopolymer treated sand. In: New frontiers in geotechnical engineering, pp 19–27

Woods SW, Balfour VN (2008) The effect of ash on runoff and erosion after a severe forest wildfire, Montana, USA. Int J Wildland Fire 17(5):535–548

Woods SW, Balfour VN (2010) The effects of soil texture and ash thickness on the post- fire hydrological response from ash-covered soils. J Hydrol 393:274–286